Field-induced Conductance Switching by Charge-state Alternation in Organometallic Single-Molecule Junctions

Florian Schwarz and Emanuel Lörtscher

IBM Research - Zurich, Säumerstrasse 4, 8803 Rüschlikon, Switzerland

Georg Kastlunger and Robert Stadler

University of Vienna, Department of Physical Chemistry, Sensengasse 8/7, 1090 Vienna, Austria and
TU Wien - Vienna University of Technology, Institute for Theoretical Physics,
Wiedner Hauptstrasse 8-10, 1040 Vienna, Austria

Franziska Lissel, Carolina Egler-Lucas, Sergey N. Semenov, Koushik Venkatesan, and Heinz Berke

Department of Chemistry, University of Zürich, Winterthurerstrasse 190, 8057 Zürich, Switzerland

Charge transport through single molecules can be influenced by the charge and spin states of redox-active metal centres placed in the transport pathway. These molecular intrinsic properties are usually addressed by varying the molecule's electrochemical and magnetic environment, a procedure that requires complex setups with multiple terminals. Here we show that oxidation and reduction of organometallic compounds containing either Fe, Ru or Mo centres can solely be triggered by the electric field applied to a two-terminal molecular junction. Whereas all compounds exhibit bias-dependent hysteresis, the Mo-containing compound additionally shows an abrupt voltage-induced conductance switching, yielding high-to-low current ratios exceeding 1000 at voltage stimuli of less than 1.0 V. DFT calculations identify a localized, redox-active molecular orbital that is weakly coupled to the electrodes and closely aligned with the Fermi energy of the leads because of the spin-polarised ground state unique to the Mo centre. This situation opens an additional slow and incoherent hopping channel for transport, triggering a transient charging effect of the entire molecule and a strong hysteresis with unprecedented high low-to-high current ratios.

Switching an electric signal from a low- to a high-current state is one of the key elements in an electric circuit with applications in signal processing, logic data manipulation or storage. In current Si-based technology with device dimensions approaching the sub-5nm range, it becomes increasingly difficult to maintain large high-to-low ratios mainly because of leakage currents. Therefore alternative switching mechanisms are needed. In single-molecule electronics, a variety of intrinsic conductance-switching mechanisms[1] exist: Gating of the molecular orbitals (MOs) by electrostatic[2] or electrochemical means[3], which requires a third electrode, or modifying specific photoactive molecular structures, e.g. by optically irradiating the molecule to form or break bonds[4–7]. Also mechanically-induced changes in the molecule–metal coupling[8] can lead to conductance alternations. Another trigger is the electric field inherently present in a molecular transport junction: Conformational changes due to interactions between the electric field and molecular dipoles were demonstrated to alternate the conductance of single-molecule junctions[9–11] by up to a factor of 70.

Potentially more powerful mechanisms exploit intrinsic molecular quantum phenomena related to spin and charge states. An early example of addressing the spin state of a single molecule[12–14] revealed Kondo resonances using cobalt (Co) metal centres[15]. More recently, a spin cross-over was induced by an electric field in iron (Fe)-based molecular nanoclusters[16] (with

high-to-low ratios of $\sim$ 2), and in a coupled spin pair of two Co atoms[17] (with high-to-low ratios of 2 - 3). Regarding intrinsic charge states, Coulomb blockade peaks were reported in ruthenium (Ru)-containing wires[18], but not confirmed in self-assembled monolayers.[19] On the single-molecule level, Ru-based molecules showed conformation-induced changes in the conductance[20] rather than changes due to intrinsic redox mechanisms. Two Ru metal centres in a photochromatic compound demonstrated reversible light-induced conductance switching in ensemble junctions.[21,22] In another study, the importance of the copper (Cu) coordination on the conductance was demonstrated[23].

Placing Individual Metal Centres in the Transport Pathway

Earlier we studied dinuclear organometallic Fe compounds with various anchoring schemes[24,25] and discovered indications of field-induced conductance switching in the case of weak molecule–metal coupling. Motivated by these findings, we have developed mononuclear organometallic compounds of the type $(MeCOSC_6H_4\text{-}C\equiv C\text{-})M(P\cap P)_2$ (M = Fe; $P\cap P$ = 1,2 - bis(diethylphosphino)ethane: (**1**); M = Ru, Mo (Molybdenum); $P\cap P$ = 1,2 -bis(diphenylphosphino)ethane: (**2**), (**3**)) using weak thiol coupling[26,27] to preserve molecule-internal spin and charge degrees of freedom for the solid-state molecular junctions. Fe, Ru and Mo were chosen as metal centres. The synthetic strategy aims at placing

the metal centres right in the transport pathway (Fig. 1a,b) to achieve an optimal influence on transport and maximum interaction with the electric field. We used identical acetylenic backbones to constrain the variable parameters to the metal centres and their ligand fields. To prevent dimerization, the sulphur end groups were acetyl-protected, with the protection groups being hydrolyzed *in situ*, forming the metal–molecule–metal junctions Au–**1'**–Au, Au–**2'**–Au, and Au–**3'**–Au (Fig. 1c). For the Fe metal centre, we used the bidentate phosphine ligands depe (depe = 1,2-bis(diethylphosphino)ethane) and for the Ru[28] and Mo centres, dppe (dppe = 1,2-bis(diphenylphosphino)ethane) chelate ligands. To extend the molecular length to 2.5 nm (S–S distance), we chose phenylene spacers as conducting backbones. The synthesis of **2** was reproduced using a previously reported procedure[28,29], whereas new synthetic protocols were established for **1** and **3** (see SI for details).

Conductance Switching in Single-Molecule Junctions

First, we perform current–voltage I–V data acquisition by repeatedly forming and breaking the junction[30] (see SI). In the entire data sets, we find a substantial number of curves ($\sim$ 90 %) that all exhibit distinct features differing from conventional non-linear molecular transport, namely, curves with hysteretic behaviour. Here, the curves acquired for sweeps from negative to positive bias are separated in a given voltage range from those acquired in the opposite direction. For the Au–**1'**–Au junction, around 85 % of the curves show hysteresis, for Au–**2'**–Au 80 %, and for Au–**3'**–Au 95 %. Fig. 1d shows 50 representative I–V curves taken at 50 K (see SI sections 10, 16-18 for statistics, sampling rate and temperature dependence). The hysteretic behaviour of the three compounds differs in the voltage range and the transition between the two envelopes. Accordingly, we categorised the I–Vs into two types: Type I curves are found for all compounds and are characterised by a small hysteresis that affects only a particular section of the voltage (blue backgrounds in Fig. 1d), whereas the I–Vs for the low- and high-bias regimes are nominally identical. The conductance gap (as defined by the onset in transport) is not altered, and the transition between the curves is continuous. Type II curves are only found for the Mo compound and differ from type I curves by an approximately 100x lower current and an abrupt switching between two distinct curves, accompanied by a hysteresis. Here, the conductance gaps change substantially (e.g. from 0.15 V to 0.85 V). Fig. 1e summarises the experiments schematically by providing also the sweep directions. When analysing the occurrences of type I and type II curves, we find that they depend on the junction configuration: Type II curves are found just before breaking the molecular junction and show a switching between two distinct states (Fig. 2a). When extracting the maximum high-to-low ratio in the hysteresis region and plotting it versus the corresponding

voltage (Fig. 2b), we find that type I curves display a narrow energy distribution, whereas type II curves seem to depend non-linearly on energy, with an increasing ratio for increasing bias. The high-to-low current ratios are 1.5 to 20 for type I switching consistently for all compounds, and exceed 1000 for type II switching.

Coherent Tunneling and Decoherent Hopping Transport

In principle, several possible explanations exist for the hysteretic curves at smaller junction distances (type I) and the abrupt switching at larger junction distances (type II): As the ground state of the Mo compound **3** and some of the excited states of the Fe compound **1** and the Ru compound **2** are magnetic, a high-spin/low-spin (HS/LS) crossover comes to mind, given the observed switching in similar systems.[16,17] There, the HS/LS crossover caused a drastic change in the electronic structure across the entire electron wavelength spectrum that accompanied the switching between two distinct electronic states. In our experimental data, however, we do not find such drastic changes, e.g. no change in the conductance gap for type I curves and almost identical curves for certain voltage regimes for both types. Moreover, the nuclei of the molecules would adapt to that and thereby preclude hysteresis simply because there is nothing that could cause a time delay. In contrast, an oxidation or reduction of the transition-metal compounds would enable a potential observation of hysteresis, as proposed theoretically.[31–33] Those authors argued that if the charging rate is similar to the bias sweeping rate, a time delay required for a memory effect could occur, making the charging visible in the I–V curves. Here, the conductance is governed by a coherent tunnelling channel mediated by a delocalized molecular orbital (MO) ("fast channel"), whereas hysteresis is related to charging of a localized MO in an electron-hopping channel ("slow channel") (Fig. 3a). The probability of the localized MO to be occupied determines the respective conductance contributions from the two charging states at every bias increase.

To simulate transport through single molecules, these charging probabilities were implemented into a stochastic approach. For calculating I–V curves, we combine proposed algorithms[33] with data from density functional theory (DFT) calculations for the transmission (defining coherent tunnelling) and the transfer integral, reorganization energy and driving force (describing electron hopping[34–36]). First, we demonstrate that by varying the ratio between the bias sweeping rate and the charging/hopping rate, the abrupt switching shown in Fig. 1c can be qualitatively reproduced for a simple two-MO tight-binding model. In Fig. 3b, we show I–V curves simulated for forward and reverse bias sweeps for various coupling strengths, γ, and fixed voltage sweeping rates, u. For the strongest coupling, $\gamma/u = 10^{12}$ V^{-1}, a statistical average of multiple switching events is observed,

and as a consequence, the forward and backward sweeps fall together with the average of the two limiting I–V curves obtained from the integration of the transmission functions of the reduced and the oxidized systems (shown as orange and gray dotted lines in Fig. 3b, respectively). When lowering the coupling to $\gamma/u = 10^4$ V^{-1}, averaging covers a smaller number of redox processes per integration time, Δt, resulting in fringes. For $\gamma/u = 100$ V^{-1}, there is roughly one jump in each integration interval, and for the weakest coupling, $\gamma/u = 0.5$ V^{-1}, only a single jump happens during a full sweep. Going from the strongest to the weakest coupling step by step (Fig. 3b), the voltage range where both sweeps follow the lower curve for low bias and the upper one for high bias becomes larger because ever higher voltages are needed to increase the likelihood of jumps. In the wide range of couplings from $\gamma/u = 10^{12}$ to 100 V^{-1}, however, the forward and backward I–V curves still follow the same path, although our stochastic approach creates uncertainties or line-thickening for ratios of γ/u smaller than 10^8 V^{-1}. Only with γ/u as low as 1 V^{-1} an irreversible switching or a "lock-in" process does take place, where the forward sweep follows the lower limiting curve for the reduced state and the backward sweep the upper one for the oxidized state; a scenario that qualitatively explains the type II curves for the Mo junction. Fig. 3c displays the hopping rates for oxidation and reduction, showing that the lower the ratio, the later R_{ox} and R_{red} cross the horizontal line defining the sweeping rate. R_{ox} determines the probability of charging the compounds, whereas the stability of this oxidized state depends inversely on R_{red}. Therefore, as can be seen from the left-hand-side panel, the bias necessary for reaching the charged state is inversely proportional to the coupling strength. R_{red}, in contrast, decreases with the coupling strength, which makes a reduction even at lower biases less likely, finally enabling the occurrence of a "lock-in" process during bias sweeps.

Let us now look at the electronic structures of the transport junctions as obtained from DFT calculations (Fig. 4). Energetic positions of the MO's and their spatial distributions as well as the corresponding transmission functions are computed by a Nonequilibrium Green's Function (NEGF) DFT formalism[37–39] with the GPAW code[40,41]. Because the Mo compound **3** is the only compound among the three with a spin-polarised ground state, we show its MO eigenenergies and transmission functions for spin-up and spin-down separately (green curves in Fig. 4a). The magnetic property of the Mo system is the reason why a very localised MO with d_{xy} symmetry on the metal atoms (where z is the transport direction) moves close to the Fermi level for one spin orientation (violet dots). In contrast, this MO lies far outside of any reasonable bias window for the Fe compound **1** and the Ru compound **2**. As a high degree of localization of a MO results in a very weak coupling to the electrodes, this MO can be considered the "slow channel" for the Mo compound, while for the Fe and Ru compounds the

	ΔG_0	λ_{in}	λ_{img}	λ_{tot}	V
Fe (Au–**1′**–Au)	0.408	0.079	-0.021	0.057	2.6×10^{-3}
Ru (Au–**2′**–Au)	0.499	0.094	-0.022	0.072	2.3×10^{-3}
Mo (Au–**3′**–Au)	0.203	0.075	-0.017	0.058	1.2×10^{-5}
Mo (+0.5 Å)	0.269	0.075	-0.013	0.062	1.3×10^{-6}

TABLE I. Parameters for electron hopping calculated from DFT for the three compounds at equilibrium geometry and for the Mo compound **3** also for a junction with the S-Au bond elongated by 0.5 Å on each side. All values are given in eV.

HOMO-1 (d_{yz}) plays this role. For all three systems, the "fast channel" is provided by the delocalized HOMO d_{xz} (Fig. 4b).

To calculate the hopping rates for the oxidation/reduction that govern the switching between neutral and charged compounds, we follow an approach developed earlier.[36] Table 1 lists all relevant parameters for both charging states for all three systems at the equilibrium distance. For the Mo compound, it also gives those values at an elongation of the bonding distance between the anchor group and the electrodes by 0.5 Å on both sides according to the experimental findings that type II curves are found for elongated junctions just before rupture. The driving force ΔG_0, which is defined by the energy difference of the "slow-channel" MO and E_F, is lower for Mo than for Fe and Ru by a factor of 2 - 3. Its transfer integral is two orders of magnitudes smaller and even three orders of magnitude smaller at the elongated distance. Because of the self-interaction problem of DFT, which becomes more severe for localized states, the calculations overestimate the spatial extension of the respective orbital and thereby also the transfer integral. Additionally, we have to account for the fact that the binding of the molecule to the metal surfaces is idealised in our DFT calculations, where we use perfectly planar Au(111) surfaces and symmetric bonding of the compounds at equilibrium distances. To account for these aspects, all calculated transfer integrals are consistently scaled down by a factor of 100 for the calculated I–V curves in the lower panels of Fig. 4c. In all panels, different sweeping rates are used for the forward and backward sweep, in agreement with the experimental situation (see SI). Whereas for the Au–**1′**–Au and the Au–**2′**–Au junctions, an elongated configuration reveals only a minor influence on the hysteresis and the functional behaviour, the Au–**3′**–Au junction shows an abrupt transition at the weaker coupling conditions induced by elongation. This situation perfectly reproduces the experimental findings in terms of switching energy, relative current levels, type of hysteresis and drastic change in the conductance gap. Furthermore, DFT calculations can also reproduce the high-to-low current ratios, which are around 1.5 - 4.5 for type I hysteresis and around 200 for type II hysteresis with abrupt switching (Fig. 4c).

Conclusion and outlook

In summary, we have experimentally and theoretically investigated the transport properties of organometallic molecules containing Fe, Ru and Mo metal centres in their transport pathway. We find hysteretic transport properties with continuous transitions for all three transport junctions, and additionally an abrupt switching for the Mo compound. Comprehensive DFT modelling, taking into account bias-driven charging, indicates an oxidation/reduction mechanism mediated by a weakly coupled, localized MO that is unique to the Mo compound because of its spin-polarized ground state. This MO gives rise to abrupt switching with high-to-low current ratios of more than 1000, outperforming all previously explored molecular-intrinsic conductance-switching mechanisms, such as magnetoresistance.[42] DFT combined with a two-channel transport model qualitatively agrees with experiments regarding the functional behaviour of the hysteresis. We therefore conclude that intrinsic redox functionality is maintained in weakly-coupled solid-state organometallic junctions, remains accessible at feasible electric fields in a two-terminal geometry, and can be controlled by tuning the voltage sweeping rate in respect to the intrinsic oxidation and reduction rates. Moreover, by bias-induced charge-state alternations, a conductance switching with technologically relevant high-to-low current ratios exceeding 1000 at voltages of 1.0 V could be achieved in a single-molecule building block. Even though technological parameters, such as fatigue, switching speed, non-volatility etc., remain to be determined in real device geometries, such ultimately scaled building blocks fulfil in principle the requirements for future memory in terms of reasonably low operational fields, speed, and large high-to-low current ratios.

[1] Van der Molen, S.J. & Liljeroth, P. Charge transport through molecular switches. *J. Phys.* **22**, 133001 (2010).

[2] Song, H. *et al.* Observation of molecular orbital gating. *Nature* **462**, 1039–1043 (2009).

[3] Liao, J. *et al.* Cyclic conductance switching in networks of redox-active molecular junctions. *Nano Lett.* **10**, 759–764 (2010).

[4] Irie, M. Diarylethenes for memories and switches. *Chem. Rev.* **100**, 1685–1716 (2000).

[5] Dulic, D. *et al.* One-way optoelectronic switching of photochromic molecules on gold. *Phys. Rev. Lett.* **91**, 207402 (2003).

[6] Kronemeijer, A.J. *et al.* Reversible conductance switching in molecular devices. *Adv. Mat.* **20**, 1467–1473 (2008).

[7] Van der Molen, S.J. *et al.* Light-controlled conductance switching of ordered metal–molecule-metal devices. *Nano Lett.* **9**, 76–80 (2009).

[8] Quek, S.Y. *et al.* Mechanically controlled binary conductance switching of a single-molecule junction. *Nature Nanotech.* **4**, 230–234 (2009).

[9] Blum, A.S. *et al.* Molecularly inherent voltage-controlled conductance switching. *Nature Mat.* **4**, 167–172 (2005).

[10] Lörtscher, E., Ciszek, J.W., Tour, J.M., Riel, H. Reversible and controllable switching of a single-molecule junction. *Small* **2**, 973–977 (2006).

[11] Meded, V., Bagrets, A., Arnold, A. & Evers, F. Molecular switch controlled by pulsed bias voltages. *Small* **5**, 2218–2223 (2009).

[12] Kahn, O. & Martinez, C. J. Spin-transition polymers: From molecular materials toward memory devices. *Science* **279**, 44–48 (1998).

[13] Sato, O., Tao, J. & Zhand, Y.-Z. Control of magnetic properties through external stimuli. *Angew. Chem. Int. Ed.* **46**, 2152–2187 (2007).

[14] Baadji, N. *et al.* Electrostatic spin crossover effect in polar magnetic molecules. *Nature Mat.* **8**, 813–817 (2009).

[15] Park, J. *et al.* Coulomb blockade and the Kondo effect in single-atom transistors. *Nature* **417**, 722–725 (2002).

[16] Prins, F., Morabal-Capilla, M., Osorio, E.A., Coronado, E. & van der Zant, H.S.J. Room-temperature electrical addressing of a bistable spin-crossover molecular system. *Adv. Mat.* **23**, 545–1549 (2011).

[17] Wagner, S. *et al.* Switching of a coupled spin pair in a single-molecule junction. *Nature Nanotech.* **8**, 575–579 (2013).

[18] Kim, B. *et al.* Temperature and length dependence of charge transport in redox-active molecular wires incorporating Ruthenium(II) bis(σ-arylacetylide) complexes. *J. Phys. Chem. C* **111**, 7521–7526 (2007).

[19] Luo, L. *et al.* Length and temperature dependent conduction of Ruthenium-containing redox-active molecular wires. *J. Phys. Chem. C* **115**, 19955–19961 (2011).

[20] Ruben, M. *et al.* Charge transport through a cardan-joint molecule. *Small* **4**, 2229–2235 (2008).

[21] Meng, F. *et al.* Photo-modulable molecular transport junctions based on organometallic molecular wires. *Chem. Sci.,* **3**, 3113–3118 (2012).

[22] Meng, F. *et al.* Orthogonally modulated molecular transport junctions for resettable electronic logic gates. *Nature Comm.* **5**, 3023 (2014).

[23] Ponce, J. *et al.* Effect of metal complexation on the conductance of single-molecular wires measured at room temperature. *J. Am. Chem. Soc.* **136**, 8314–8322 (2014).

[24] Schwarz, F. *et al.* High-conductive organometallic molecular wires with delocalized electron systems strongly coupled to metal electrodes. *Nano Lett.* **14**, 5932–5940 (2014).

[25] Lissel, F. *et al.* Organometallic single-molecule electronics: Tuning electron transport through (diphosphine)$_2$FeC$_4$Fe(diphosphine)$_2$ building blocks by varying the molecule–metal anchoring scheme from coordinative to covalent. *J. Am. Chem. Soc.* **136**, 14560–14569 (2014).

[26] Reed, M.A., Zhou, C.; Muller, C.J., Burgin, T.P. & Tour, J.M. Conductance of a molecular junction. *Science* **278**, 252–254 (1997).

[27] Zotti, L.A. *et al.* Revealing the role of anchoring groups in the electrical conduction through single-molecule junctions. *Small* **6**, 1529–1535 (2010).

[28] Wuttke, E. *et al.* Divinylphenylene- and ethynylvinylphenylene-bridged mono-, di- , and triruthe-

nium complexes for covalent binding to gold electrodes. *Organometallics* **33**, 4672–4686 (2014).

29 Touchard, D. *et al.* Vinylidene-, Alkynyl-, and *trans*-bis(alkynyl)ruthenium complexes. crystal structure of *trans*-[Ru(NH₃)(C≡C-Ph)(Ph₂PCH₂CH₂PPh₂)₂]PF₆. *Organometallics* **16**, 3640–3648 (1997).

30 Lörtscher, E., Weber, H.B. & Riel, H. Statistical approach to investigating transport through single molecules. *Phys. Rev. Lett.* **98**, 176807 (2007).

31 Galperin, M., Ratner, M. & Nitzan, A. Hysteresis, switching, and negative differential resistance in molecular junctions: A polaron model. *Nano Lett.* **5**, 125–130 (2005).

32 Kuznetsov, A.M. Negative differential resistance and switching behavior of redox-mediated tunnel contact. *J. Chem. Phys* **127**, 084710 (2007).

33 Migliore, A. & Nitzan, A. Irreversibility and hysteresis in redox molecular conduction junctions. *J. Am. Chem. Soc.* **135**, 9420–9432 (2013).

34 Kastlunger, G. & Stadler, R. Charge localization on a redox-active single-molecule junction and its influence on coherent electron transport. *Phys. Rev. B* **88**, 035418 (2013).

35 Kastlunger, G. & Stadler, R. Density functional theory based calculations of the transfer integral in a redox-active single-molecule junction. *Phys. Rev. B* **89**, 115412 (2014).

36 Kastlunger, G. & Stadler, R. A density functional theory based direct comparison of coherent tunnelling and electron hopping in redox-active single molecule junctions. *Phys. Rev. B* **91**, 125410 (2015).

37 Brandbyge, M., Mozos, J.-L., Taylor, J. & Stokbro, K. Density-functional method for nonequilibrium electron transport *Phys. Rev. B* **65**, 165401 (2002).

38 Xue, Y., Datta, S. & Ratner, M.A. First-principles based matrix Green's function approach to molecular electronic devices: General formalism. *Chem. Phys.* **281**, 151–170 (2002).

39 Rocha, A.R. *et al..* Towards molecular spintronics. *Nature Mater.* **4**, 335–339 (2005).

40 Mortensen, J.J., Hansen, L.B. & Jacobsen, K.W. Real-space grid implementation of the projector augmented wave method. *Phys. Rev. B* **71**, 035109 (2005).

41 Enkovaara, J. *et al.* Electronic structure calculations with GPAW: A real-space implementation of the projector augmented-wave method. *J. Phys.* **22**, 253202 (2010).

42 Schmaus, S. *et al.* Giant magnetoresistance through a single molecule. *Nature Nanotech.* **6**, 185–189 (2011).

Acknowledgements

Author contribution

Additional information

Competing financial interests

The authors declare no competing financial interests.
Chemical Synthesis. The synthetic steps and full characterisation of all compounds can be found in the supporting information.

Transport measurements. Electron-beam-structured break junctions are mechanically actuated in a three-point bending mechanism operated under ultra-high-vacuum conditions (UHV; pressure $p < 2 \times 10^{-9}$ mbar) at 50 K.[30] Molecules are deposited from a highly diluted solution in dry tetrahydrofuran (THF; 4×10^{-5} m/L). Electrical characterization is carried out with a Hewlett-Packard Semiconductor Parameter Analyzer HP4156B upon repeated opening and closing of the molecular junction (more details can be found in the supporting information).

Computational details. All calculations of transmission probabilities $T(E)$ and $I–V$ curves were performed within a NEGF-DFT framework[37−39] with the GPAW code.[40,41] We chose a linear combination of atomic orbitals (LCAO) on a Double Zeta level with polarisation functions (DZP) for the basis set and a Perdew-Burke-Ernzerhof (PBE) parametrisation for the exchange-correlation (XC) functional. The MO eigenenergies were calculated by decoupling the basis functions localised on the molecule from those of the surface states via a subdiagonalisation of the transport Hamiltonian.[34]

For the redox process, we combine a recent formalism[33] with a coherent tunnelling description based on NEGF-DFT for the calculation of the $I–V$ characteristics of the reduced and oxidized states and a hopping description of the redox reaction based on Marcus theory[36]. By calculating the bias-dependent reaction rates of oxidation and reduction, a probability P can be determined that describes the system's probability to be in one of the respective charge states after a given integration time Δt. To simulate single $I–V$ sweeps, we apply a stochastic approach, in which we trap the system into one distinct charge state in every step. By calculating the change of probability dP, defined by either $dP = R_{ox}dt$ or $dP = R_{red}dt$, between two time steps t and $t+dt$, where $dt \ll \Delta t$, and comparing dP defined in this way with a random number between 0 and 1, we create a criterion for the switching between the two states. The overall current is then calculated from a mean value $I(V) = \frac{1}{n}\sum_{i=1}^{n} I(V,i)$, averaging over all n current values, with $\Delta t = n * dt$. More details can be found in the supplementary information.
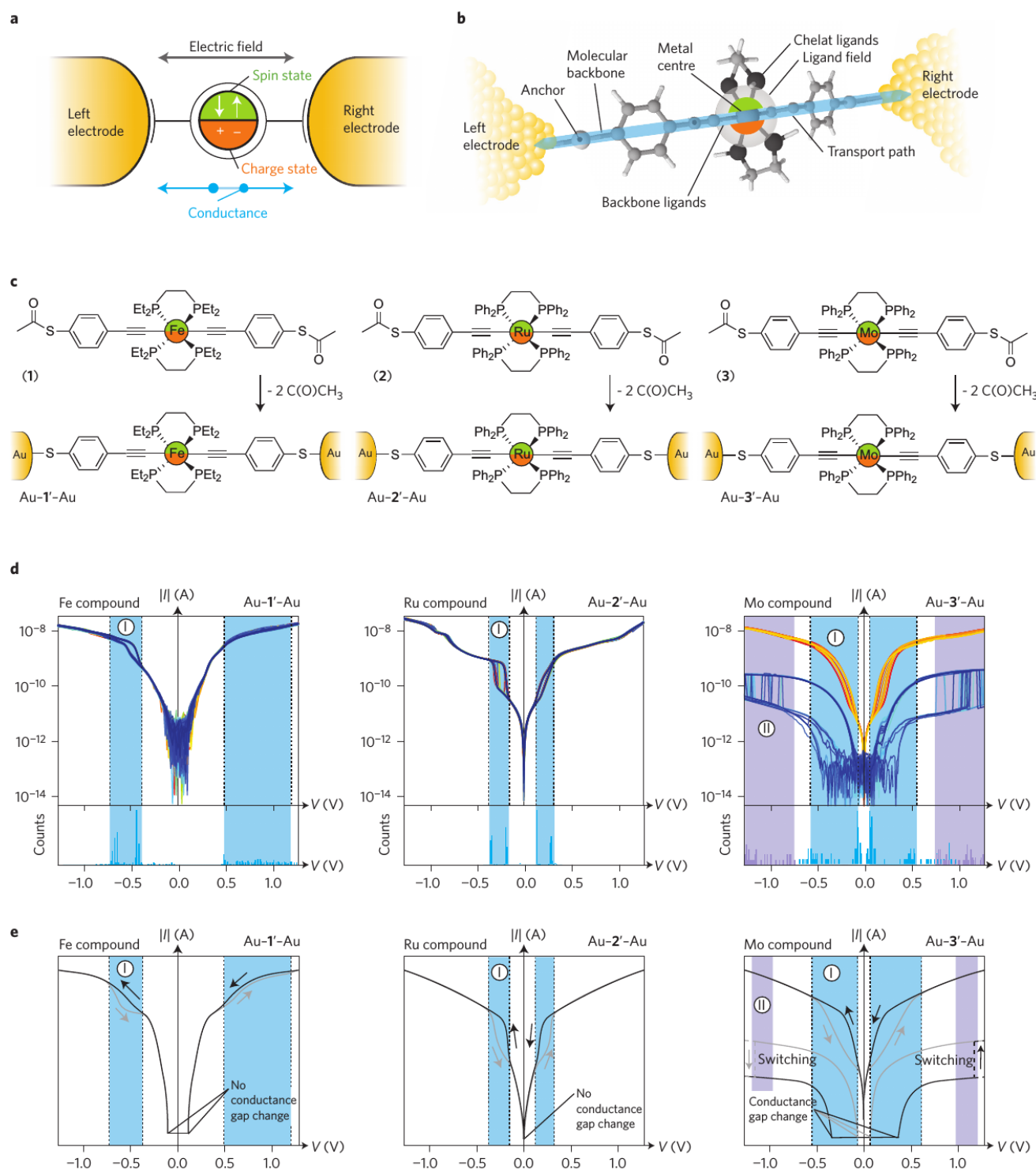
FIG. 1. **Organometallic single-molecule junctions bearing Ru, Fe and Mo metal centres to provide charge and spin degrees of freedom. a**, Addressing spin (green) and charge (orange) states of a molecular junction by the electric field present by means of the bias applied in a two-terminal geometry. **b**, Anatomy of the organometallic molecular junction with one metal centre placed directly in the charge-transport pathway. **c**, Mononuclear compounds of type *trans*-(MeCOSC$_6$H$_4$-C≡C-)M(P∩P)$_2$ (M = Fe; P∩P = 1,2 - bis(diethylphosphino)ethane: (**1**); M = Ru, Mo; P∩P = 1,2 -bis(diphenylphosphino)ethane: (**2**), (**3**)). Shown are also the representative transport junctions Au–**1**′–Au, Au–**2**′–Au, and Au–**3**′–Au, respectively. **d**, 50 representative I–V characteristics taken at 50 K: The Fe **1** and Ru compounds **2** both show a continuous splitting of the I–Vs, providing a hysteresis region (blue background). Here, no change in the conductance gap or in the high-bias conductance is found. The same type of curves (labelled I) is found also for the Mo compound **3** with a slightly larger hysteresis regime. In addition, there is a second type of curves (labelled II) that reveals an abrupt switching accompanied by a large change in the conductance gap (violet background). **e**, Schematic representation of the two types of hysteresis with continuous I (Fe, Ru and Mo compounds **1**, **2**, and **3**) and abrupt switching II (Mo compound **3** only).
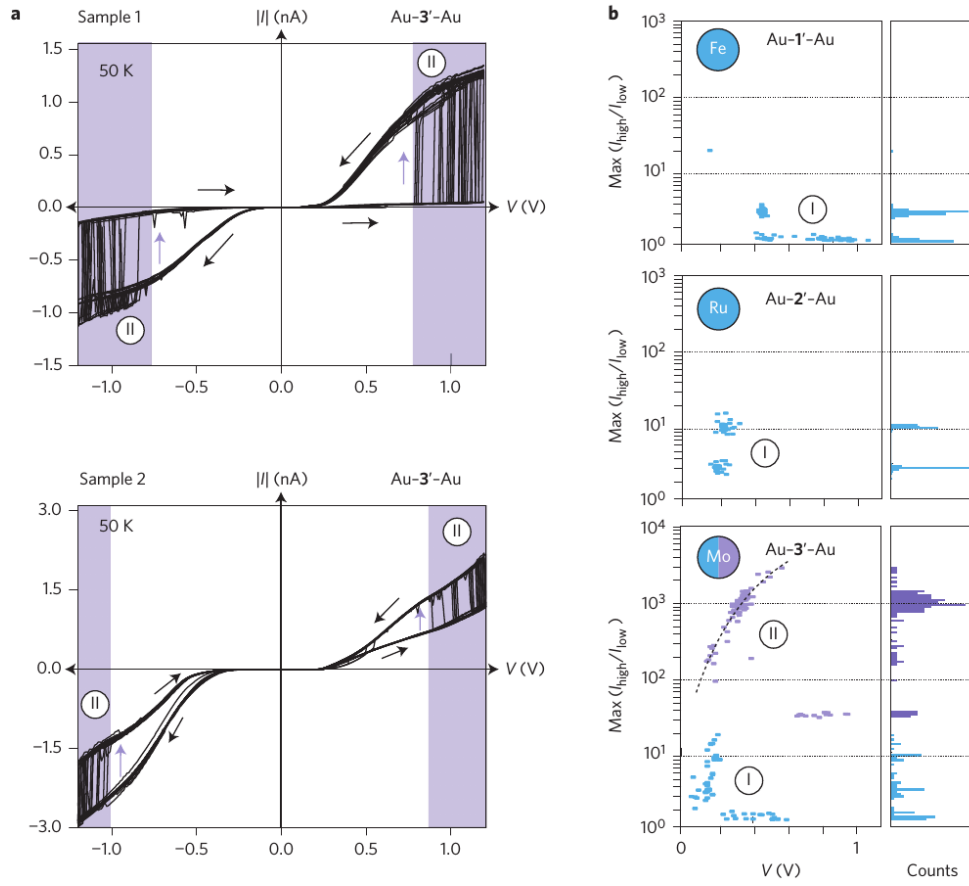
FIG. 2. **High-to-low current ratios for type *I* and type *II* curves**. **a**, Type *II* hysteretic curves on linear current scale found for the Mo junction Au–**3′**–Au, revealing an abrupt switching from a low- to a high-conductance regime (50 K). Plotted are two data sets measured on fully independent samples with typical differences for single-molecule experiments regarding the current amplitude and switching voltages. **b**, Statistics on maximum high-to-low current ratios extracted in the hysteresis regime for type *I* and type *II* curves for all compounds. Whereas type *I* ratios vary from 1.5 (Fe compound **1**) to 20 (Mo compound **3**), the type *II* switching found only for the Mo compound **3** attains 2500 at a bias of less than 0.6 V. The ratio seems to follow a voltage dependence as indicated by the black dotted line.
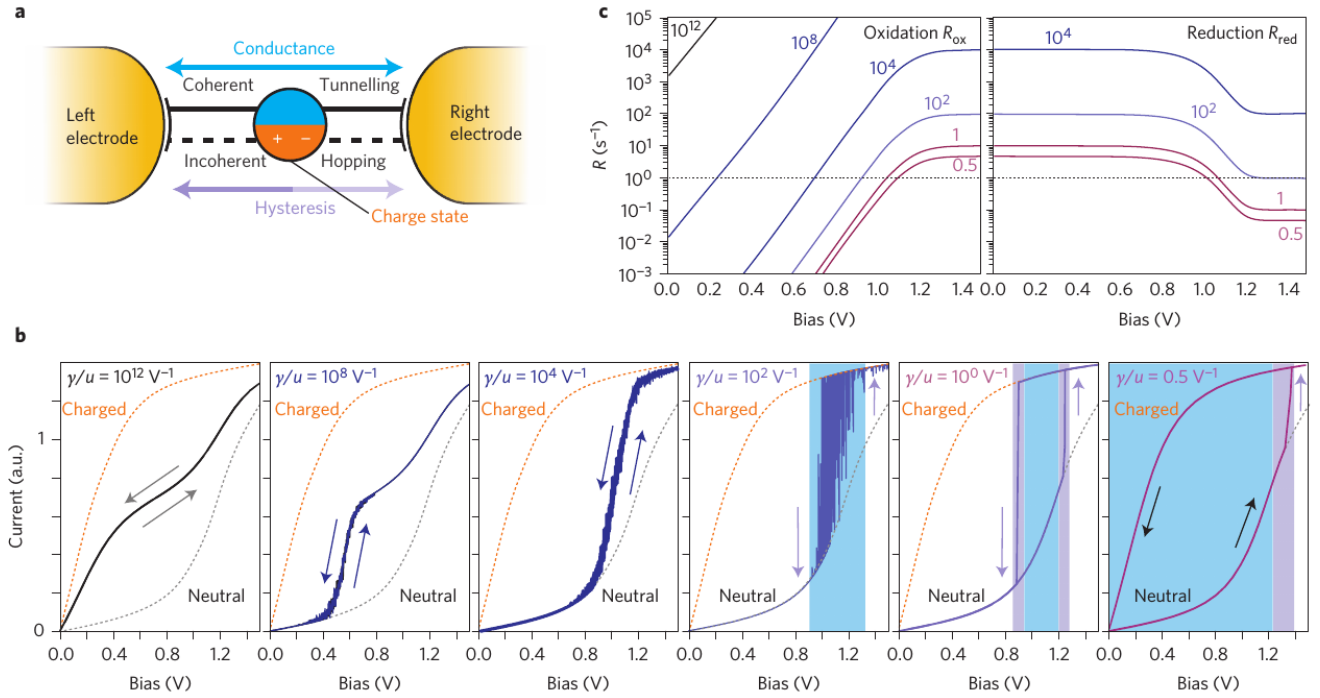
FIG. 3. **Two-channel transport mechanism in single-molecule junctions and its influence on current switching and hysteresis**. **a**, Model for a two-channel transport mechanism through a molecular junction with a fast coherent tunnelling path (cyan) responsible for the conductance, and a slow, incoherent hopping path (violet) causing hysteresis, e.g., by charging. **b**, Calculated I–V curves from a 2-state tight-binding model, with one strongly and one weakly coupled molecular orbital (MO). The parameters used in this model are $\Delta E_{ox/red} = 0.1$ eV for the localized MO, a reorganization energy of 0.1 eV and a bias sweep rate of 1 V/s; the onsite energies for the delocalized MO in the neutral and the charged system are set to -0.6 eV and -0.1 eV, respectively. The driving force ΔG_0 of the reaction depends on both $\Delta E_{ox/red}$ and the average bridge population in the fast channel.[33] In our calculations, the bias sweeping rate determines the integration time, Δt, between two voltages, whereas the hopping rate for both oxidation and reduction is defined by the square of the same MO-metal-coupling Γ, or the super exchange rates $\gamma = \frac{2\pi}{\hbar}\Gamma^2$, which thereby determines the number of hopping processes from the reduced to the oxidized state and vice versa that occur within Δt. The current follows a monotonous trace between neutral (dotted line) and charged (orange line) state for $\gamma/u \geq 10^4$ V^{-1}, but the I–V characteristics reveals a bistable range for decreasing rates that finally leads to hysteresis (blue background) and an abrupt switching for rates around 1 (violet background indicates abrupt switching regimes). **c**, Corresponding reaction rates for oxidation, R_{ox}, and reduction, R_{red}, as a function of bias and different ratios of the coupling strength, γ, and the bias sweeping rate, u.
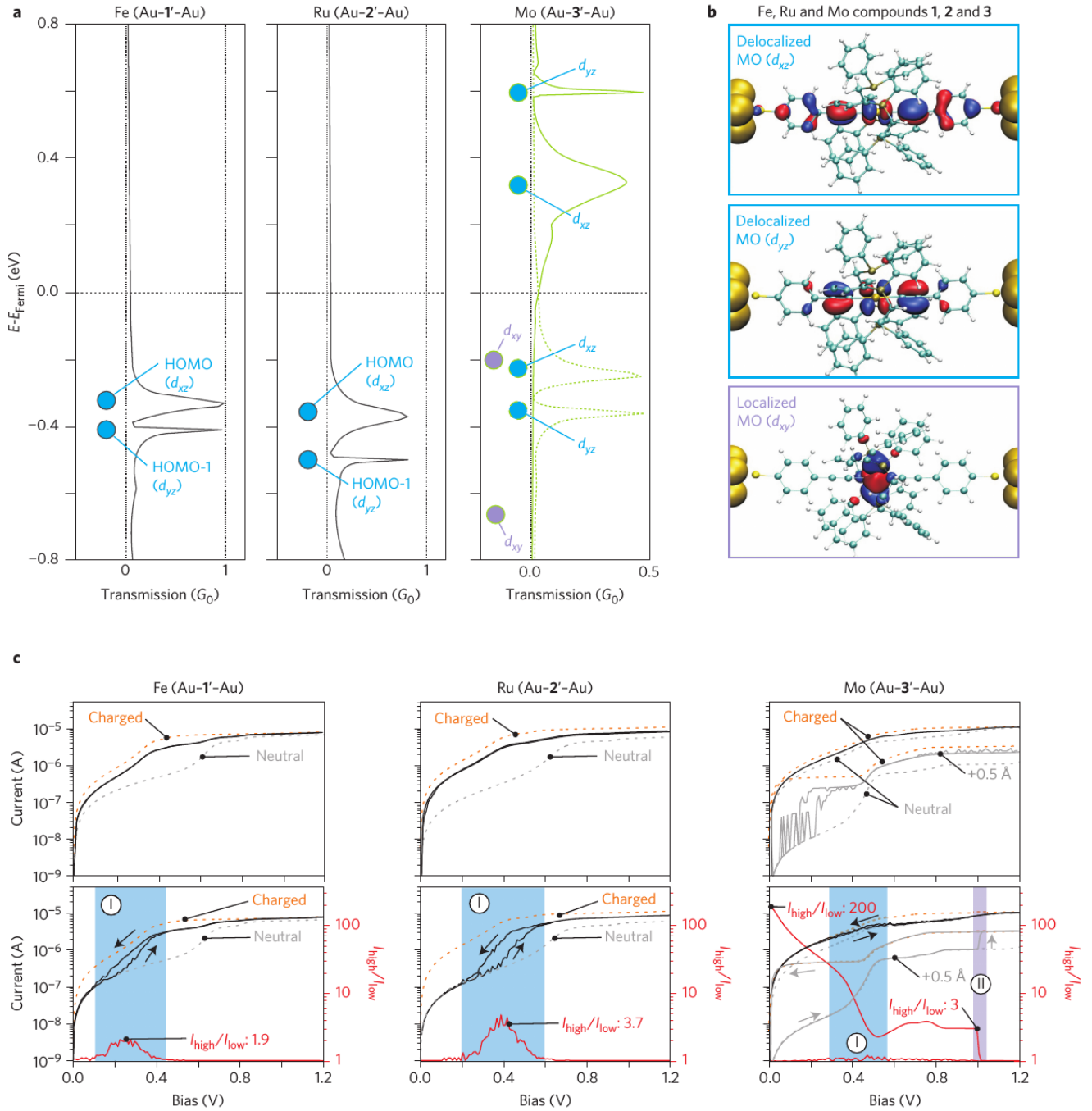
FIG. 4. **DFT-derived transmission and molecular orbitals as well as transport characteristics calculated under finite bias**. **a**, Total transmission functions (grey and green curves) and selected MO eigenenergies (dots) with respect to $E_{F,Au}$ obtained from a sub-diagonalization of the transport Hamiltonian, and the respective transmission functions calculated with NEGF-DFT; the two are plotted separately for spin-up and spin-down electrons for the Mo compound **3** because of the latter's spin-polarized ground state (green lines). **b**, Spatial distributions of the MOs with the delocalized HOMO and HOMO-1 and a localized MO (with d_{xy} symmetry) found only for the Mo compound to lie in the relevant energy window. **c**, I–V curves calculated by a NEGF-DFT approach combined with a hopping description for the charging of the slow channel[36] by using the hysteresis formalism[33]. The upper three panels show uncorrected I–V curves using the parameters given in Table 1, whereas for the calculations in the lower panels, the transfer integral is scaled down by a factor of 100 for reasons given in the main text. Only for the Mo compound **3** a weaker coupling results in the abrupt switching curves. The red curves provide the ratio between high and low currents for the two types of hysteresis. All I–V curves were simulated from 100 bias steps in each direction with integration times of 0.01 s for the forward and 0.1 s for the backward sweeps.